Inorganic Chemistry

Article

pubs.acs.org/IC

Synthesis and Electrocatalytic Water Oxidation by Electrode-Bound Helical Peptide Chromophore–Catalyst Assemblies

Derek M. Ryan,[§] Michael K. Coggins,[§] Javier J. Concepcion,[‡] Dennis L. Ashford, Zhen Fang, Leila Alibabaei, Da Ma, Thomas J. Meyer,* and Marcey L. Waters*

Department of Chemistry, University of North Carolina at Chapel Hill, Chapel Hill, North Carolina 27599, United States

Supporting Information

ABSTRACT: Artificial photosynthesis based on dye-sensitized photoelectrosynthesis cells requires the assembly of a chromophore and catalyst in close proximity on the surface of a transparent, high band gap oxide semiconductor for integrated light absorption and catalysis. While there are a number of approaches to assemble mixtures of chromophores and catalysts on a surface for use in artificial photosynthesis based on dye-sensitized photoelectrosynthesis cells, the synthesis of discrete surface-bound chromophore–catalyst conjugates is a challenging task with few examples to date. Herein, a versatile synthetic approach and electrochemical characterization of a series of oligoproline-based light-harvesting chromophore–water-oxidation catalyst assemblies is described. This approach combines solid-phase peptide synthesis for systematic variation of the backbone, copper(I)-catalyzed azide–alkyne cycloaddition (CuAAC) as an orthogonal approach to install the chromophore, and assembly of the water-oxidation catalyst in the final step. Importantly, the catalyst was found to be incompatible with the conditions both for amide bond formation and for the CuAAC reaction. The modular nature of the synthesis with late-stage assembly of the catalyst allows for systematic variation in the spatial arrangement of light-harvesting chromophore and water-oxidation catalyst and the role of intrastrand distance on chromophore–catalyst assembly properties. Controlled potential electrolysis experiments verified that the surface-bound assemblies function as water-oxidation electrocatalysts, and electrochemical kinetics data demonstrate that the assemblies exhibit greater than 10-fold rate enhancements compared to the homogeneous catalyst alone.

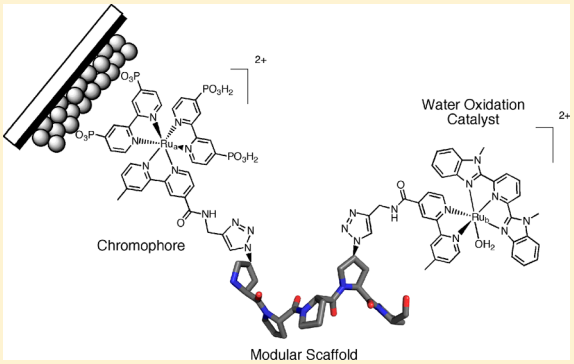

INTRODUCTION

Artificial photosynthesis based on dye-sensitized photoelectrosynthesis cells (DSPECs) is an attractive route for the storage of solar energy in chemical bonds. The development of efficient DSPECs would help to alleviate current issues arising in solar energy supply and storage arising from the inability of conventional PV devices to function at night or under poor lighting conditions. Chemical fuels from DSPECs can be stored for later use on demand by combustion or in fuel cells.

The principal components behind an efficient DPSEC device are a transparent, high band gap oxide semiconductor and a surface-bound, light-harvesting chromophore–catalyst assembly for integrated light absorption and catalysis.[1] Light absorption and injection by the chromophore is followed by intra-assembly electron transfer activation of the catalyst.[1]At a photoanode for water oxidation, the water-oxidation catalyst is activated by intra-assembly electron transfer to the oxidized chromophore as a means of transferring the redox equivalents necessary for water oxidation. The transfer rate of the oxidative equivalent from the oxidized chromophore to the catalyst needs to effectively compete with the rate of back electron transfer from the semiconductor surface in order to drive water oxidation.

Several strategies have been investigated for the assembly of both chromophores and catalysts on metal-oxide surfaces, including codeposition,[2,3] electropolymerization,[4,5] and self-assembly.[6] However, a limitation of these approaches is a lack of control of chromophore–catalyst spacing, orientation, and distance from the surface due to the lack of discrete assembly architectures. One strategy to address the issue of separating the oxidized catalyst from the semiconductor surface is to synthesize chromophore–catalyst assemblies that link the light-harvesting chromophore and water-oxidation catalyst while maximizing the separation distance from the catalyst to the semiconductor surface to slow back electron transfer.[1,7−9] To date, several chromophore–catalyst assemblies have been reported that use Ru(II) polypyridyl chromophores for efficient light absorption with various direct linkage strategies to a remote water-oxidation catalyst.[10−17] The chromophores can be synthetically tailored to include phosphonated bipyridine (pbpy) ligands, which facilitate attachment to oxide surfaces.[12−14,16,17] The need to develop a new synthetic approach for each new system, however, has inhibited systematic studies

Received: May 16, 2014
Published: July 21, 2014

dx.doi.org/10.1021/ic5011488 | Inorg. Chem. 2014, 53, 8120–8128

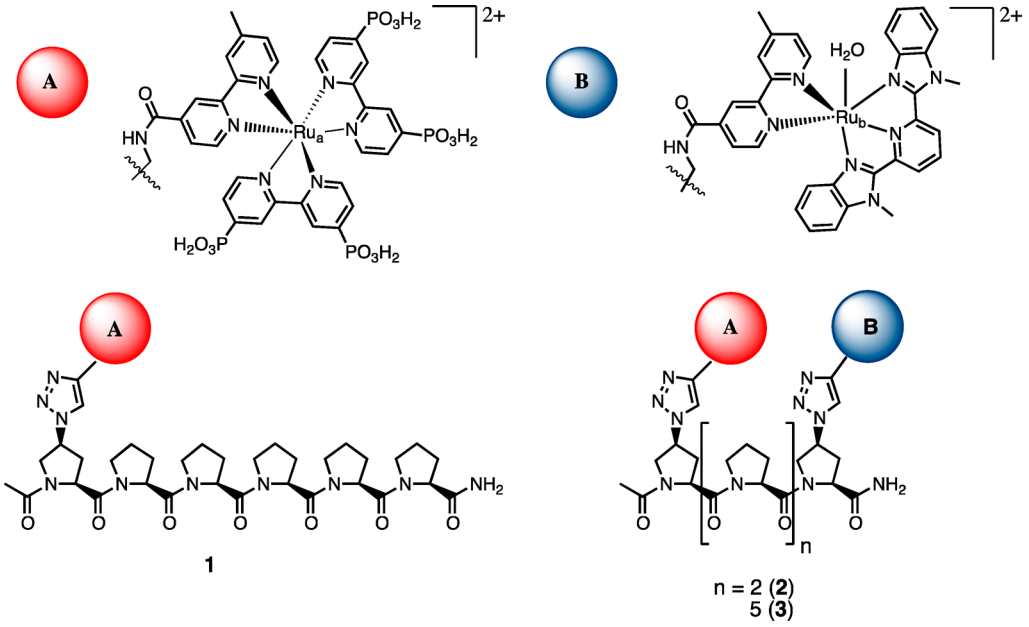

Figure 1. Chemical structures of metallopeptides **1**–**3**, with **A** (red sphere) representing chromophore $[Ru(pbpy)_2(L)]^{2+}$ and **B** (blue sphere) representing water-oxidation catalyst $[Ru(Mebimpy)(bpy)OH_2]^{2+}$.

of the effect of structural variation on the optimization of assembly properties.

An alternative to the direct linking between chromophore and catalyst is to use a modular approach with a rigid scaffold for linking the chromophore and catalyst. Such an approach has been used before for multiple chromophore assemblies, but not for combinations of chromophores and catalysts. In our effort to apply our previous approach for multiple chromophore assemblies to chromophore–catalyst assemblies, we found that a new synthetic strategy was required. We report here the use of a rigid oligoproline peptide as a modular scaffold that incorporates both a light-harvesting chromophore and water-oxidation catalyst using a combination of solid-phase peptide synthesis (SPPS),[18] the copper-catalyzed alkyne–azide cycloaddition reaction (CuAAC, or "click" reaction) (Figure 1), and late-stage catalyst assembly.[19−22] Importantly, we found that neither SPPS nor CuAAC is compatible with the water-oxidation catalyst. Instead, attachment of the bpy ligand to the scaffold, followed by formation of the catalyst in the final step, is required. A significant advantage of this strategy is the ease of preparation, the ability to vary both chromophores and catalysts, and the ability to control the interspatial distance between the chromophore and catalyst by incorporating a predetermined number of proline spacers. Finally, while oligoprolines are used as the scaffold in this work, the scaffold itself can also be varied using different natural or unnatural amino acid building blocks, making the entire assembly modular in nature.

The synthesis and structural characterization of two polyproline chromophore–catalyst assembles provide a basis for exploring the effect of proline spacer units between the chromophore and catalyst on assembly properties. In this Article, we describe surface binding of these assemblies to the surface of oxide electrodes and an investigation of electrocatalytic water oxidation. Our results point to an increase in the rate of water oxidation for both polyproline assemblies at pH 1.0 by more than an order of magnitude compared to $[Ru(Mebimpy)(bpy)(H_2O)]^{2+}$ under identical conditions. There is little kinetic difference between assemblies, consistent with rapid intra-assembly electron transfer even through five intervening proline spacers.

EXPERIMENTAL SECTION

General Methods. All chemical reagents and solvent were purchased from commercial vendors and used without further purification. Synthetic protocols for *cis*-Fmoc-4-N_3-Pro, 4,4′-bis-(diethylphosphonomethyl)-2,2′-bipyridine, and 2,6-bis(1-methylbenzimidazol-2-yl)pyridine are provided in the Supporting Information. Planar fluorine-doped tin oxide (FTO) glass slides (R_s = 7–8 Ω) were purchased from Sigma-Aldrich. Prior to assembly binding, each planar FTO electrode was washed twice with neat CH_3OH, followed by 0.1 M HNO_3, water, and finally dried. GC analyses were performed on a Varian 450-GC with molecular sieve columns and a thermal conductivity detector. ^1H and ^{13}C NMR spectra were recorded at 400 and 100 MHz, respectively. High-resolution and low-resolution mass spectra were obtained using a Bruker Biotof instrument. Electrochemical measurements were performed with a model CHI660D electrochemical workstation (CH instruments) and a three-electrode system consisting of a planar fluorine-doped tin oxide working electrode (typical area 1.0–1.2 cm^2), a platinum wire counter electrode, and either a Ag/AgCl (3.5 M NaCl) or an SCE reference electrode without *i*R compensation. All potentials are referenced to the normal hydrogen electrode. Milli-Q water (>18 MΩ) was used for the preparation of all buffers and solutions. Surface binding of each assembly on planar FTO was performed by immersion of a clean planar FTO glass slide in aqueous loading solutions containing 500 μM assembly and 0.1 M $HClO_4$. Surface coverage values (Γ) were calculated by determining the charge passed (Q) under the Ru_b(III/II) CV wave and the area of the electrode (A) using the equation $\Gamma = Q/nFA$, where n is the number of electrons passed (1 e^-) and F is Faraday's constant. UV–vis spectra of each surface immobilized assembly were recorded on a Thermo Scientific NanoDrop 2000 spectrometer. Controlled potential electrolysis experiments were conducted with a closed three-compartment electrolysis cell with ∼10–12 mL of total electrolyte volume and ∼3 mL of total headspace above the working electrode cell compartment that had been deoxygenated for 30 min with N_2. Samples of each assembly in water (5 μL of 150 μM complex) were applied to the sample stage, and spectra were collected at 25 °C. Circular dichroism spectra were recorded on an applied photophysics chirascan plus steady-state

dx.doi.org/10.1021/ic5011488 | Inorg. Chem. 2014, 53, 8120–8128

circular dichroism spectrometer. Samples of complexes were diluted to 25 μM in either 0.1 M $HClO_4$, pH 3.0, 100 mM phosphate buffer, or pH 7, 100 mM phosphate buffer. Each spectrum was collected at 25 °C.

General Protocols for Solid-Phase Peptide Synthesis. Oligoproline peptides were synthesized on Rink-amide resin using Fmoc-protected amino acids. Fmoc-proline (commercially available) or *cis*-Fmoc-4-N_3-Pro (**9**) were coupled in the appropriate positions. The amide coupling reagents 2-(1*H*-benzotriazole-1-yl)-1,1,3,3-tetramethyl-uronium hexafluorophosphate (HBTU, 4 equiv) and hydroxybenzotriazole (HOBt, 3.9 equiv) were mixed with the appropriate amino acid along with *N*,*N*,*N*-diisopropylethyl amine (10 equiv) in DMF and coupled with resin. After each coupling step, a 20% piperidine in DMF solution was used to deprotect the *N*-terminal Fmoc groups. All peptides were capped with acetic anhydride prior to cleavage. Peptides were then cleaved from resin with 95:2.5:2.5 TFA/triisopropylsilane/water. Solvent was removed, and product was precipitated with diethyl ether. The product was filtered and purified by reverse phase HPLC using an Atlantis Prep OBD C-18 semipreparative column, with a gradient of 0−100% solvent B over 60 min, where solvent A was 95:5 water/MeCN, 0.1% TFA, and solvent B was 95:5 MeCN/water, 0.1% TFA. Purified samples were lyophilized, and the peptide sequences were confirmed by ESI-MS.

General Protocol for the Copper(I)-Catalyzed Azide−Alkyne Cycloaddtion (CuAAC) Reaction. For both on-resin and solution-phase CuAAC reactions, the following protocols were used. Cu(II)SO_4 (4 equiv) and sodium ascorbate (4 equiv) were stirred in 10 mM phosphate buffer (pH 8) for 5−10 min. The alkyne (1 equiv) was then added and stirred for 5 min. The solution was then added to the azide-containing peptide, which was either on resin or in solution. The CuAAC reaction mixture was stirred for 12−24 h. The on-resin CuAAC reaction was washed several times with DI H_2O and DMF to remove excess copper and unreacted ligand and then cleaved from the resin as described above. Solution-phase reactions were desalted by sephadex size-exclusion chromatography. The peptides were then purified by HPLC, as described in the peptide protocols.

Ac-(N_3-Pro$_1$)-Pro$_2$-Pro$_3$-(bpy-Pro$_4$)-Pro$_5$-Pro$_6$-CO_2NH_2 (7). This peptide was synthesized using the general protocols for solid-phase peptide synthesis described above with the following exceptions. Upon coupling *cis*-Fmoc-4-N_3-Pro, the resin was submitted to CuAAC conditions in the presence of ligand **6**. Following the click reaction, the peptide sequence was completed, acetyl-capped, and cleaved. The peptide was purified by HPLC as previously described and lyophilized. ESI-MS $[M]^+$ calcd. 975.46, found 975.48.

Synthesis of Ac-(Chromophore A-Pro$_1$)-Pro$_2$-Pro$_3$-(bpy-Pro$_4$)-Pro$_5$-Pro$_6$-CO_2NH_2 (8). Solution-phase CuAAC of chromophore **A** and **7** was conducted using the previously described CuAAC protocols. Upon completion of the reaction, excess copper and unreacted ligand were removed by sephadex size-exclusion chromatography. The peptide was purified by RP-HPLC, yielding **8**. ESI-MS $[M + 2Na]^{2+}$ calcd. 1003.343, found 1003.48. $[M + K + H_2O]^{3+}$ calcd. 672.25, found 672.15.

Synthesis of Ac-(Chromophore A-Pro$_1$)-Pro$_2$-Pro$_3$-(Catalyst B-Pro$_4$)-Pro$_5$-Pro$_6$-CO_2NH_2 (2). Peptide **8** (1 equiv) and $[Ru(Mebimpy)OTf_2]_2$ (0.5 equiv) were dissolved in a 95% ethanol:water mixture and reacted in a microwave oven at 150 °C for 20 min. Completion of the reaction was confirmed by UV−vis spectroscopy, and the solvent was removed by rotary evaporation. The product was purified by LH-20 sephadex size-exclusion chromatography, yielding the desired metallopeptide assembly **2**. ESI-MS (80% MeCN:H_2O, 1% CO_2H_2) $[M]^{4+}$ calcd. 604.55, found 604.30. $[M + 2Na + H_2O]^{2+}$ calcd.1248.86, found 1248.61. $[M]^{2+}$ calcd. 1208.98, found 1208.61.

Synthesis of Ac-(Chromophore A-Pro$_1$)-Pro$_{2-4}$-(Catalyst B-Pro$_5$)-Pro$_{6-9}$-$CONH_2$ (3). The peptide was synthesized as described in the general methods. The water-oxidation catalyst **B** was installed as previously for **2**. Briefly, the peptide portion (1 equiv) and $[Ru(Mebimpy)OTf_2]_2$ (0.5 equiv) of **3** were dissolved in a 95% ethanol:water mixture and reacted in a microwave oven at 150 °C for 20 min. Completion of the reaction was confirmed by UV−vis spectroscopy, and the solvent was removed by rotary evaporation. The product was purified by LH-20 sephadex size-exclusion chromatography, yielding the desired metallopeptide assembly **3**. Product was confirmed by observing fragmentation in the ESI-MS, as outlined in Scheme S1 (Supporting Information). ESI-MS (80% MeCN:H_2O, 1% CO_2H_2) for **14** $[M + Na]^+$ calcd. 986.77, found 986.5. ESI-MS (80% MeCN:H_2O, 1% CO_2H_2) for **15** $[M - H + Na]^+$ calcd. 1051.02, found 1051.93. ESI-MS (80% MeCN:H_2O, 1% CO_2H_2) for **16** $[M + 2CO_2H_2]^+$ calcd. 844.19, found 844.94.

Synthesis of Ac-(Chromophore A-Pro$_1$)-Pro$_{2-5}$-(Catalyst B-Pro$_6$)-Pro$_{7-9}$-$CONH_2$ (4). The peptide was synthesized as described in the general methods. The water-oxidation catalyst **B** was installed as previously for **2**. Briefly, the peptide portion (1 equiv) and $[Ru(Mebimpy)OTf_2]_2$ (0.5 equiv) of **3** were dissolved in a 95% ethanol:water mixture and reacted in a microwave oven at 150 °C for 20 min. Completion of the reaction was confirmed by UV−vis spectroscopy, and the solvent was removed by rotary evaporation. The product was purified by LH-20 sephadex size-exclusion chromatography, yielding the desired metallopeptide assembly **4**. Product was confirmed by observing fragmentation in the ESI-MS. ESI-MS (80% MeCN:H_2O, 1% CO_2H_2) for **17** $[M + Na]^+$ calcd. 986.5, found 986.77. ESI-MS (80% MeCN:H_2O, 1% CO_2H_2) for **15** $[M - H + Na]^+$ calcd. 1051.02, found 1051.93. ESI-MS (80% MeCN:H_2O, 1% CO_2H_2) for **16** $[M + 2CO_2H_2]^+$ calcd. 844.19, found 844.94.

Synthesis of Ac-(Chromophore A-Pro$_1$)-Pro$_{2-6}$-(Catalyst B-Pro$_7$)-Pro$_{8-9}$-$CONH_2$ (5). The peptide was synthesized as described in the general methods. The water-oxidation catalyst **B** was installed as previously for **2**. Briefly, the peptide portion (1 equiv) and $[Ru(Mebimpy)OTf_2]_2$ (0.5 equiv) of **3** were dissolved in a 95% ethanol:water mixture and reacted in a microwave oven at 150 °C for 20 min. Completion of the reaction was confirmed by UV−vis spectroscopy, and the solvent was removed by rotary evaporation. The product was purified by LH-20 Sephadex size-exclusion chromatography, yielding the desired metallopeptide assembly **5**. Product was confirmed by observing fragmentation in the ESI-MS. ESI-MS (80% MeCN:H_2O, 1% CO_2H_2) for **18** $[M]^+$ calcd. 986.5, found 986.77. ESI-MS (80% MeCN:H_2O, 1% CO_2H_2) for **15** $[M - H + Na]^+$ calcd. 1051.02, found 1051.93. ESI-MS (80% MeCN:H_2O, 1% CO_2H_2) for **16** $[M + 2CO_2H_2]^+$ calcd. 844.19, found 844.94.

RESULTS AND DISCUSSION

System Design. Chromophore−catalyst metallopeptide assemblies were designed to investigate their potential for electrocatalytic water oxidation (Figure 1). We chose to use a polyproline scaffold as it is known to adopt a relatively rigid helical structure (PPII helix) in water that aligns the *i* and *i* + 3 positions on the same side of the helix at a distance of approximately 9 Å, providing a means for controlling the distance between the chromophore and catalyst.[23−28] Metallopeptide **1** is a control peptide that has been previously reported by our laboratory and bears the known phosphonated light-harvesting chromophore **A** at the *N*-terminal position (*i* position).[29] The target was to synthesize metallopeptide **2**, containing chromophore **A** at the same *N*-terminal position (*i*) and water-oxidation catalyst $[Ru(Mebimpy)(bpy)OH_2]^{2+}$ (**B**)[30−32] in the fourth position (*i* + 3), thus positioning the chromophore and catalyst on the same side of the helix, in close proximity, as supported by MD simulations of a similar peptide containing two chromophores at *i* and *i* + 3 positions.[29] In peptide **3**, the chromophore and catalyst are placed at the *i* and *i* + 6 positions with a distance between attachment points of approximately 18 Å.[29]

Synthesis. Metallopeptide **1** had previously been synthesized by a combination of solid-phase peptide synthesis and the CuAAC catalyzed click reaction.[29] The peptide portion of **1** was synthesized on Rink amide resin using standard fluorenylmethoxycarbonyl (Fmoc) protection and deprotection protocols. The peptide was synthesized using Fmoc-proline (Pro), with

dx.doi.org/10.1021/ic5011488 | Inorg. Chem. 2014, 53, 8120−8128

Scheme 1. Synthesis of Complex 2[a]

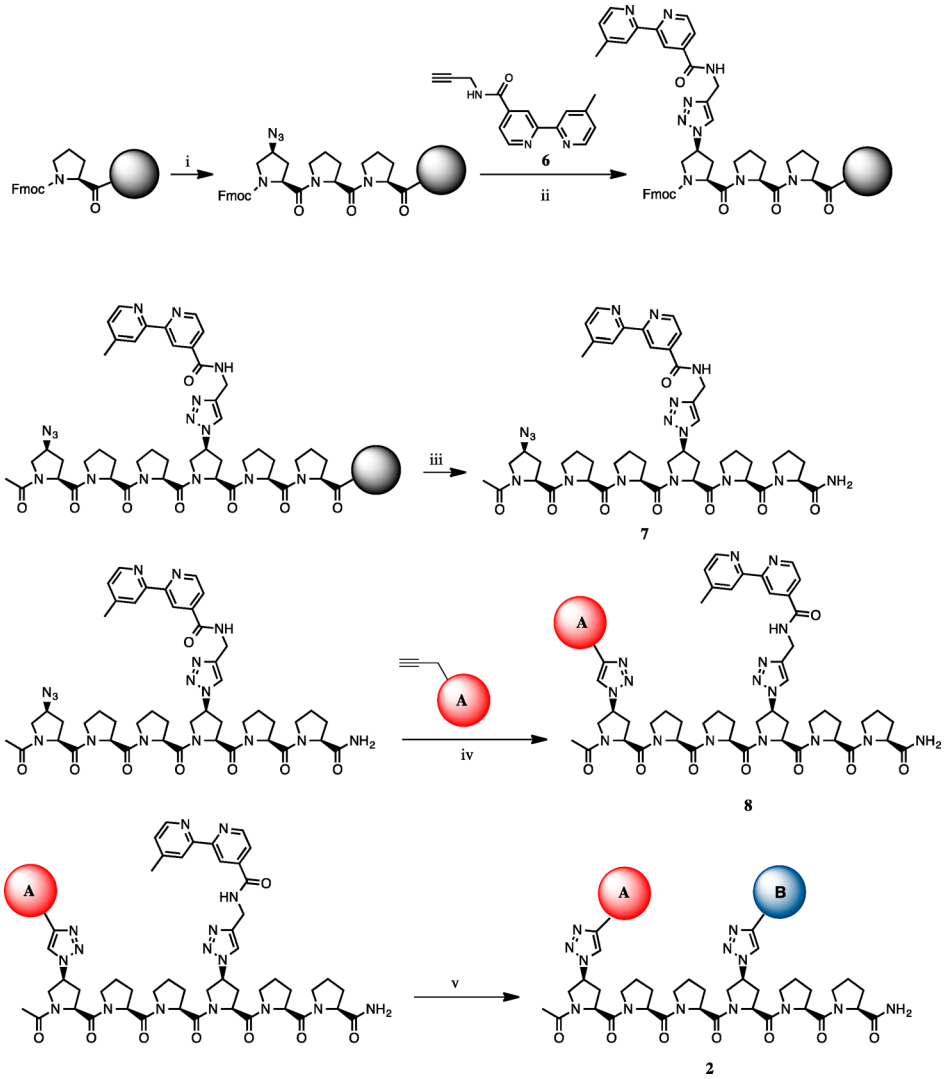

[a]Synthesis conditions: (i) Fmoc-Pro (or Fmoc-4-N_3-Pro), HBTU, HOBt, DMF, DIPEA. (ii) CuAAC = Cu(II)SO_4, sodium ascorbate, DMF. (iii) TFA, H_2O, TMS. (iv) Cu(II)SO_4, sodium ascorbate, 10 mM phosphate buffer (pH 8). (v) [Ru(Mebimpy)$(OTf)_2]_2$ ethanol:water (3:1), microwave 130 °C.

the exception of the *N*-terminal position in which a Fmoc-*cis*-4-N_3-Pro was incorporated. Following completion of the peptide, chromophore **A** was clicked to the backbone, giving the desired metallopeptide **1**.

Initial attempts to synthesize complex **2** followed a similar strategy as complex **1**, namely, utilizing CuAAC for the sequential attachment of both the water-oxidation catalyst and chromophore **A.** Peptide synthesis up to the first azidoproline was completed, followed by an on-resin CuAAC reaction to an alkyne-functionalized catalyst at the *i* + 3 position. Peptide synthesis was then completed with azidoproline incorporated at the *N*-terminal position. The peptide was then cleaved from the resin, followed by the final CuAAC reaction to the chromophore at the *N*-terminal azidoproline. In all cases, these reactions only resulted in the formation of complex mixtures containing unreacted starting material or unidentifiable products. An amide coupling strategy to the water-oxidation catalyst was then explored through inclusion of *cis*-4-NH_2-Pro at the *i* + 3 position of the peptide, and the requisite *N*-terminal azide for the CuAAC reaction to the chromophore. All attempts at coupling the free amine on the peptide to a derivatized Mebimpy ligand bearing a carboxylic acid led to exceptionally low yields (<5%) and complex mixtures. It was hypothesized that the open coordination site on the catalyst was responsible for coupling reagent or product degradation, resulting in poor amide coupling yields.

On the basis of these results, and due to the orthogonality and reliability of the CuAAC reaction, a novel approach to the synthesis of complex **2** was designed (Scheme 1). In this scheme, the azide required for the attachment of the catalyst to the peptide backbone was effectively protected by CuAAC reaction with and alkyne-substituted uncoordinated 2,2′-bipyridine ligand at the *i* + 3 position. This feature would allow for elongation of the peptide backbone on solid phase and inclusion of the *N*-terminal azide for the attachment of the chromophore at the *i* position. The water-oxidation catalyst could then be constructed by using the uncoordinated bpy ligand on the peptide backbone in the final step of the synthesis, thus avoiding both the click and the amide coupling reactions in the presence of active catalyst.

dx.doi.org/10.1021/ic5011488 | *Inorg. Chem.* 2014, 53, 8120−8128

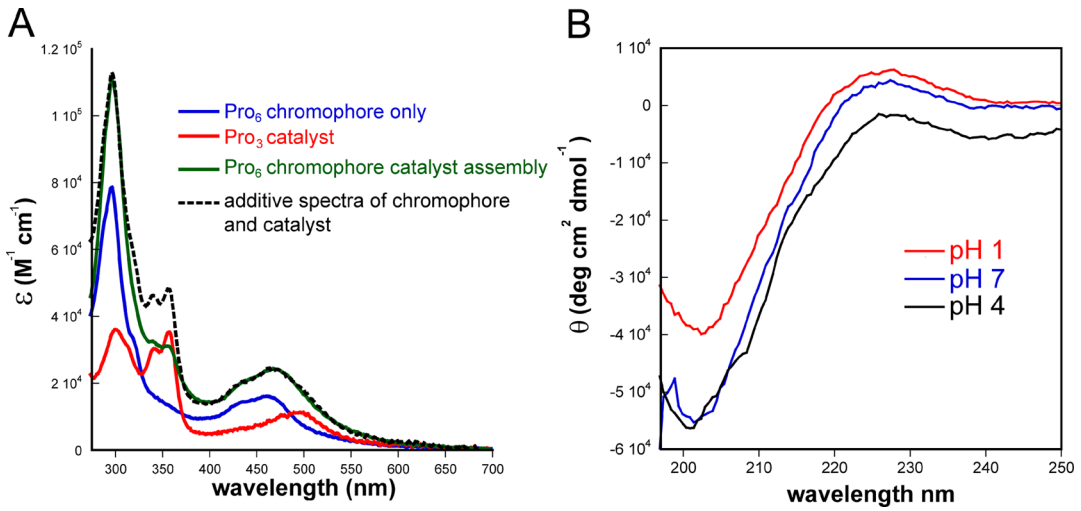

Figure 2. (A) Ground-state absorption spectra of **1** (blue) and **2** (green) in aqueous 0.1 M $HClO_4$ and **B** (red) in 70% ethylene carbonate and 30% water (1% triflic acid). All spectra were background-subtracted in their respective solvents and obtained at 25 °C. The additive spectrum of **1** and catalyst **B** is shown in black. (B) CD spectra of metallopeptide **2** (25 mM) in pH 1 (0.1 M $HClO_4$, red), pH 4 (10 mM phosphate, blue), and pH 7 buffer (10 mM phosphate, black).

The peptide backbone was sequentially assembled from the *C*-terminus using standard Fmoc coupling conditions through the $i + 3$ position, which acts as the site of attachment for the water-oxidation catalyst. At this position, *cis*-Fmoc-4-N_3-Pro was incorporated into the peptide backbone, followed by an on-resin CuAAC coupling to 4′-methyl-(2,2′-bipyridine)-4-propargyl amide (**6**). Upon completion of the CuAAC reaction, the peptide was further elaborated with two additional Fmoc-Pro residues and *N*-terminated with *cis*-Fmoc-4-N_3-Pro at the i position. This was followed by acetyl capping of the peptide, cleavage from the resin with TFA, and purification by HPLC. The purified peptide **7** was submitted to a CuAAC reaction with chromophore **A**, yielding **8**. The metallopeptide was then purified by HPLC and reacted with $[Ru(Mebimpy)(OTf)_2]_2$ under microwave irradiation to install the water-oxidation catalyst possessing a triflate counterion that was immediately hydrolyzed *in situ* to **B**, giving the desired complex **2**.

The general route for synthesis of assembly **3** was identical to that for **2** with the exception of inclusion of five proline spacers instead of two (Figure 1). This peptide was synthesized to investigate the effect of chromophore−catalyst spacing on the rate of oxidative equivalent transfer. The ability to utilize this methodology to rapidly vary the chromophore−catalyst assemblies has a distinct advantage over methods involving direct linkage of the chromophore and catalyst, for which a unique synthesis for each assembly would be required.

Spectroscopic and Structural Characterization. Metallopeptides **1** and **2** were characterized by UV−vis spectroscopy and circular dichroism (CD) spectroscopy (Figure 2 and the Supporting Information, Figures S1 and S2). Solution-phase UV−vis measurements on **1** displayed a metal-to-ligand charge-transfer absorption (MLCT) from 400−500 nm (Figure 2A). The UV spectrum of **2** included a $\pi \rightarrow \pi^*$ absorption from the Mebimpy ligand at 325−370 nm and an MCLT band from 400−510 nm. Control experiments using a peptide fragment bearing three proline residues and the water-oxidation catalyst were also characterized by UV−vis spectroscopy. The spectra of the water-oxidation catalyst displayed a red-shifted MLCT absorption (450−550 nm) relative to the chromophore. When the spectra of **1** and the water-oxidation catalyst were superimposed, the resulting spectra closely resembled that observed for complex **2**. These results are consistent with previously reported complexes assembled from a similar $Ru(pbpy)_2(bpy)^{2+}$-derived chromophore and $Ru(Mebimpy)(bpy)^{2+}$-derived catalysts.[12−14] The spectrum of assembly **3** was similar to the spectrum for assembly **2** (Figure S1, Supporting Information).

To determine if **2** and **3** adopt the desired PP II helix in solution, CD spectra of each as a function of pH were acquired. PP II helices possess characteristic CD spectra with a minimum at 205−210 nm and a maximum at 220 nm. The CD spectra of **1** with increasing pH clearly indicate a PP II helix at all pH values, consistent with spectra previously reported for this complex.[23,24,33,34] The CD spectra of **2** and **3** with increasing pH are also consistent with a well-folded PP II structure from pH 1−7 (Figure 2 and Figure S2, Supporting Information).[25−28] The differences in the magnitude of the CD spectrum at pH 1 relative to pH 4 and pH 7 may be due to a slight decrease in folding, although contributions from this effect do not appear in the electrochemical properties of the assembly. In a previous study, it was demonstrated that a related polyproline peptide bearing two light-harvesting chromophores retained the PP II secondary structure when bound to metal-oxide surfaces.[23]

Surface Electrochemistry. Cyclic voltammetry (CV) experiments were conducted with phosphonate surface-bound chromophore−catalyst assemblies **2** and **3** on planar fluorine-doped tin oxide (FTO) electrodes with a Ag/AgCl (3.5 M NaCl) reference electrode and a platinum wire counter electrode. Assembly-bound FTO electrodes (FTO-**2** and FTO-**3**: FTO-$[Ru_a^{II}\text{-}Ru_b^{II}\text{-}OH_2]^{4+}$) were prepared by soaking electrodes in 0.1 M $HClO_4$ stock solutions of each respective assembly for 12 h, resulting in saturation coverage of $\sim 1 \times 10^{-10}$ mol/cm^2 as determined by the integrated area under the anodic (oxidative) component of Ru_b(III/II) CV waves for the FTO-$[Ru_a^{II}\text{-}Ru_b^{III}\text{-}OH_2]^{5+}$/FTO-$[Ru_a^{II}\text{-}Ru_b^{II}\text{-}OH_2]^{4+}$) couple at 0.713 V vs NHE (0.1 M $HClO_4$, 0.4 M $LiClO_4$). A representative CV for FTO-**2** at pH 1.0 (0.1 M $HClO_4$) is shown in Figure 3 and exhibits waves for the FTO-$[Ru_a^{II}\text{-}Ru_b^{III}\text{-}OH_2]^{5+}$/FTO-$[Ru_a^{II}\text{-}Ru_b^{II}\text{-}OH_2]^{4+}$, FTO-$[Ru_a^{II}\text{-}Ru_b^{IV}{=}O]^{4+}$/

dx.doi.org/10.1021/ic5011488 | Inorg. Chem. 2014, 53, 8120−8128

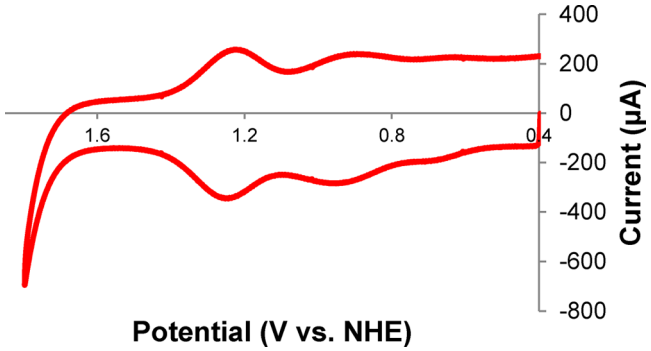

Figure 3. Cyclic voltammogram of FTO-**2** at 250 mV/s (0.1 M $HClO_4$, 0.4 M $LiClO_4$, 23 °C).

FTO-$[Ru_a^{II}$-Ru_b^{III}-$OH_2]^{5+}$, and FTO-$[Ru_a^{III}$-Ru_b^{IV}=$O]^{5+}$/FTO-$[Ru_a^{II}$-Ru_b^{IV}=$O]^{4+}$ couples with half-wave potentials ($E_{1/2}$) of 0.71, 1.16, and 1.24 V (vs NHE), respectively. The peak current of each wave was found to vary linearly with the scan rate (ν), as expected for surface-immobilized redox couples.[35] These values are consistent with those previously reported for surface-bound $[Ru(4,4'\text{-}(PO_3H_2)_2(bpy)_3]^{2+}$ and $[Ru(Mebimpy)(4,4'\text{-}(PO_3H_2)_2bpy)(H_2O)]^{2+}$.[17,36] A reversible wave for the FTO-$[Ru_a^{III}$-Ru_b^{V}=$O]^{6+}$/FTO-$[Ru_a^{III}$-Ru_b^{IV}=$O]^{5+}$ couple is not observed due to the onset of water oxidation.[36] CVs of surface-immobilized assembly FTO-**3** displayed nearly identical redox behavior to that of FTO-**2**, which is expected given the structural and electronic similarities between the two assemblies (Figure S3, Supporting Information).

Oxidation of the aqua-based catalyst in the assemblies occurs by sequential proton-coupled electron transfer (PCET) steps with oxidation of -Ru_b^{II}-OH_2^{2+} to -$Ru_b^{V}(O)^{3+}$, resulting in the pH-dependent redox behavior shown in the pH−$E_{1/2}$ (Pourbaix) diagram for FTO-**2** in Figure 4. The catalyst Ru_b(III/II) couple is pH-independent between pH 1 and 2.24, consistent with the FTO-$[Ru_a^{II}$-Ru_b^{III}-$OH_2]^{5+}$/FTO-$[Ru_a^{II}$-Ru_b^{II}-$OH_2]^{4+}$ couple. From pH 2.24 to pH 10, this wave exhibits a pH dependence of 56 mV/pH unit, consistent with the 59 mV/pH unit slope predicted by the Nernst equation and the $1e^-/1H^+$ couple FTO-$[Ru_a^{II}$-Ru_b^{III}-$OH]^{4+}$/FTO-$[Ru_a^{II}$-Ru_b^{II}-$OH_2]^{4+}$ with pK_a = 2.24 for -Ru_b^{III}-OH_2^{3+}. The catalyst Ru_b(IV/III) wave displays pH-dependent behavior from pH 1 to 2.24 with a slope of 124 mV/pH unit, consistent with a $1e^-/2H^+$ process and close to the predicted slope of 118 mV/pH unit and the FTO-$[Ru_a^{II}$-Ru_b^{IV}=$O]^{4+}$/FTO-$[Ru_a^{II}$-Ru_b^{III}-$OH_2]^{5+}$ couple (Figure 4). From pH 2.4 to 10, the dependence decreases to 68 mV/pH unit, consistent with the $1e^-/1H^+$ FTO-$[Ru_a^{II}$-Ru_b^{IV}=$O]^{4+}$/FTO-$[Ru_a^{II}$-Ru_b^{III}-$OH]^{4+}$ couple.

It is notable that the pH dependences of both the -Ru_b^{IV}=O^{2+}/-Ru_b^{III}-OH_2^{3+} and -Ru_b^{IV}=O^{2+}/-Ru_b^{III}-OH^{2+} couples are higher than predicted based on Nernstian behavior, as observed earlier for observations for surface-bound $[Ru(bpy)_{3-n}(PO_3H_2\text{-}CH_2\text{-}bpy)_n]^{2+}$, with n = 1−3 and for $[((PO_3H_2\text{-}CH_2)\text{-}bpy)_2Ru_a(bpy\text{-}NH\text{-}CO\text{-}trpy)Ru_b(bpy)(OH_2)]^{4+}$.[14,37] Also, as observed earlier, the nominally pH-independent chromophore Ru_a(III/II) wave (FTO-$[Ru_a^{III}$-Ru_b^{IV}=$O]^{5+}$/FTO-$[Ru_a^{II}$-Ru_b^{IV}=$O]^{4+}$) is slightly pH-dependent from pH 1 to 6.5, decreasing by 18 mV/pH due to local electric field effects.[14,38−41]

Water Oxidation Electrocatalysis. To determine if the surface-bound chromophore−catalyst assemblies were capable of functioning as water-oxidation electrocatalysts, controlled potential electrolysis (CPE) and scan-rate-dependent CV measurements were conducted at pH 1 (0.1 M $HClO_4$, 0.4 M $LiClO_4$) using fully loaded FTO-**2** and FTO-**3** electrodes. Sampling of the headspace from CPE measurements conducted at an applied potential of 1.74 V vs NHE (570 mV overpotential) and subsequent analysis by gas chromatography/mass spectrometry revealed the formation of 8 μmol of O_2 (~8000 turnovers, 64% Faradaic efficiency, TOF = 0.28 s^{-1}) over 8 h of electrolysis, verifying that the surface-bound assemblies are functional water-oxidation catalysts (Figure 5). No evidence for electrolysis products other than O_2 was obtained in this study. The background detection of oxygen was found to result from leakage of atmospheric O_2 into the

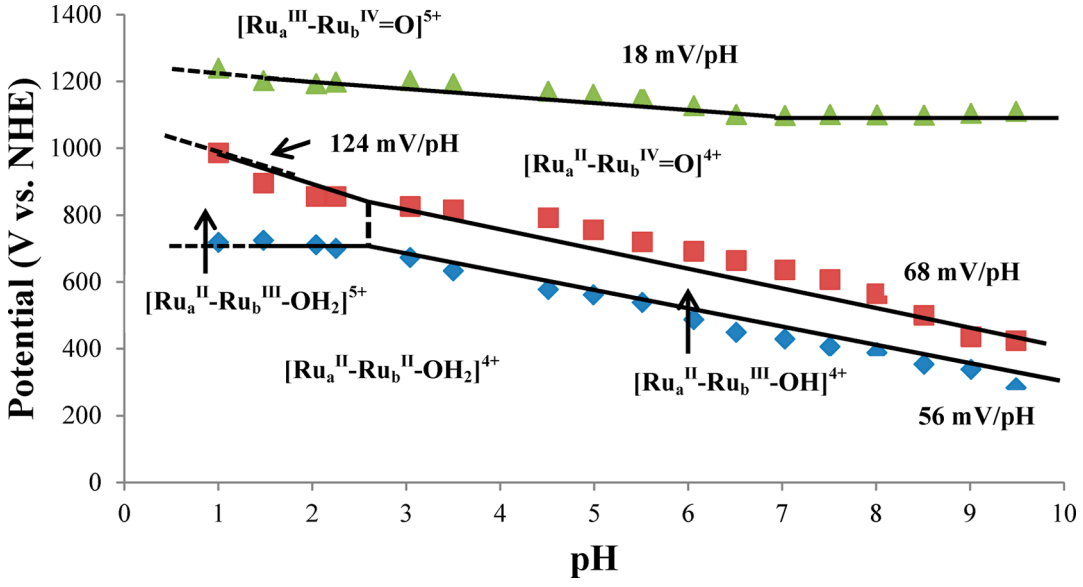

Figure 4. Pourbaix diagram for FTO-**2**. Blue data points are $E_{1/2}$ values for the FTO-Ru_a(II)-Ru_b(III/II) couple, red data points are for the FTO-Ru_a(II)-Ru_b(IV/III) couple, and green data points are for the FTO-Ru_a(III/II)-Ru_b(IV)) couple.

dx.doi.org/10.1021/ic5011488 | Inorg. Chem. 2014, 53, 8120−8128

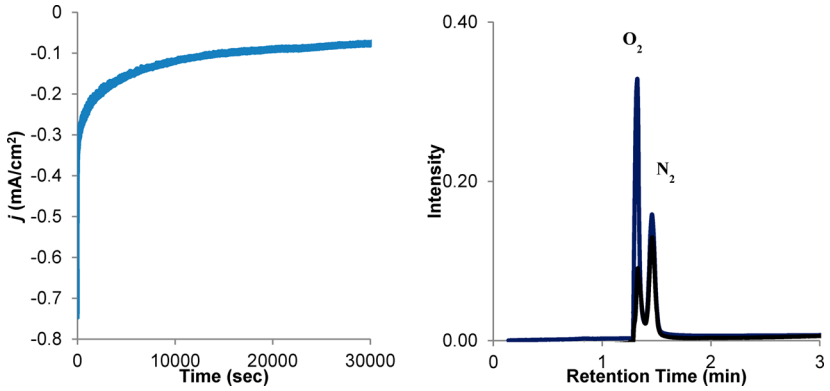

Figure 5. (Left) Electrolysis of FTO-**2** at 1.74 V vs NHE at pH 1.0 (0.1 M $HClO_4$, 0.4 M $LiClO_4$), $\Gamma = 1.1 \times 10^{-10}$ mol/cm^2. (Right) Gas chromatographic response for O_2 evolution during electrolysis (blue trace) and background response in the absence of catalyst (black trace).

electrolysis vessel over the extended period of each experiment (Figure 5).

The results of scan-rate-dependent CV measurements on both FTO-**2** and FTO-**3** in 0.1 M $HClO_4$ with 0.4 M $LiClO_4$ at room temperature were used to determine water oxidation rate constants by application of eq 1.[35] In eq 1, i_{cat} is the catalytic peak current at 1.74 V, i_p is the peak current for the -Ru_b^{III}-OH_2^{3+}/-Ru_b^{II}-OH_2^{2+} wave at $E_{1/2}$ = 0.71 V vs NHE, k_{cat} is the catalytic rate constant, ν is the scan rate in mV/s, R is the ideal gas constant, T is the temperature, n_{cat} (=4) is the number of electrons involved in water oxidation, n_p (=1) is the number of electrons involved in the oxidation of FTO-$[Ru_a^{II}$-Ru_b^{II}-$OH_2]^{4+}$ to FTO-$[Ru_a^{II}$-Ru_b^{III}-$OH_2]^{5+}$, and F is Faraday's constant.

$$i_{cat}/i_p = (4RTn_{cat}/n_p^2F)k_{cat}(\nu)^{-1} \quad (1)$$

Peak current ratios as a function of the inverse of the scan rate according to eq 1 are shown in Figures S4 and S5 (Supporting Information). From these data, k_{cat} values of 0.85(3) and 0.57(2) s^{-1} were determined for FTO-**2** and FTO-**3**, respectively. Steady-state current densities for FTO-**2** and FTO-**3** from chronoamperometric experiments are both ~0.1 mA/cm^2, which is consistent with the close k_{cat} values determined from the CV kinetics measurements. Notably, these experimental rate constants are more than an order of magnitude higher than the value reported under the same conditions for the $[Ru(Mebimpy)(bpy)(H_2O)]^{2+}$ water-oxidation catalyst (0.027 s^{-1}).[30] These results point to a redox mediator effect with the oxidized, Ru(III), chromophore accelerating the rate of water oxidation. Related observations have been reported in other chemically linked chromophore–catalyst assemblies.[14,37,42,43] The slight decrease in water oxidation rate for FTO-**3** is presumably due to a micro-environmental effect with the remote catalyst further from the electrode surface.

The results of the electrochemical experiments show that, in both redox potentials and water oxidation rates, there are only small differences between assemblies, FTO-**2** and FTO-**3**, which is not a surprise given the common catalyst. The oxidation mechanism for related, single-site oxidants in solution and on oxide surfaces is illustrated in Scheme 2 for the surface-bound, single-site catalyst $[Ru(Mebimpy)(4,4'$-$(CH_2PO_3H_2)_2$-$bpy)(H_2O)]^{2+}$.[31,32] It involves stepwise PCET oxidation of -Ru_b^{II}-OH_2^{2+} to -Ru_b^{IV}=O^{2+}, followed by further oxidation to -$Ru_b^{V}(O)^{3+}$ and rate-limiting O atom transfer to a water molecule to give a hydroperoxide intermediate, -Ru_b^{III}-OOH^{2+}. The hydroperoxide intermediate undergoes further oxidation

Scheme 2. Electrode-Immobilized Single-Site Water Oxidation Mechanism[32,44]

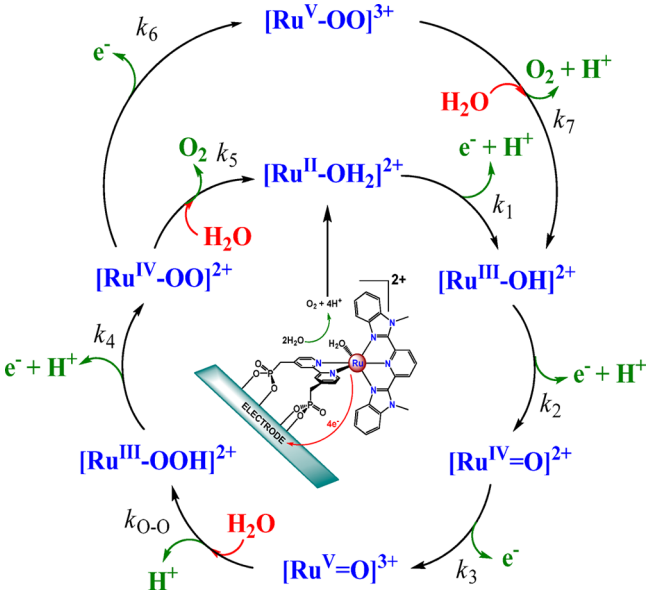

and O_2 release and re-enters the catalytic cycle. As for the surface-bound analogue shown in Scheme 2, $[Ru(Mebimpy)$-$(4,4'$-$(CH_2PO_3H_2)_2bpy)(H_2O)]^{2+}$, there is also independent evidence for the appearance of the proposed Ru–peroxide intermediates in the chromophore–catalyst assembly reported here.[32,44] Following oxidative scans through the catalytic water oxidation wave, new waves appear for Ru–peroxide couples at $E_{1/2}$ = 530 mV and 320 vs NHE. These waves were also observed when the assembly-bound electrodes are dried in air. The results of ultrafast photophysical measurements describing the interfacial dynamics following excitation and injection will be reported elsewhere.[29]

CONCLUSIONS

We describe here a novel synthetic approach applicable to the rapid synthesis of a series of light-harvesting chromophore–water oxidation assemblies, in which the chromophore is first coupled to the backbone and the water-oxidation catalyst is then assembled in the final step. The polypeptide backbone adopts a polyproline type II helix structure, which serves as a scaffold to align the two complexes along one face of the helix. This represents a significant advantage over other molecular

dx.doi.org/10.1021/ic5011488 | Inorg. Chem. 2014, 53, 8120–8128

assembly approaches in that key intra-assembly properties, including both composition and spacing, can be varied systematically and applied generally to other amide-linked scaffolds for optimization of assembly properties. Electrochemical studies have elucidated redox potentials and their associated pH dependences and demonstrated that they are relatively unaffected by binding to the surface. Water-oxidation catalysis is also maintained for the surface-bound assemblies with the assembly-based catalysts undergoing water oxidation unchanged through many turnovers. There is a notable order of magnitude rate enhancement for water oxidation by the assemblies compared to the substituent single-site, surface-bound catalyst, providing evidence for a redox mediator effect. Our results are important in demonstrating the use of standard peptide synthesis coupled with click chemistry to prepare a platform for a family of chromophore−catalyst assemblies for potential DSPEC applications.

■ ASSOCIATED CONTENT

Supporting Information

Additional synthetic details, UV/vis spectra, CD spectra, representative cyclic voltammograms of **FTO-3**, and i_c/i_p versus ν^{-1} plots for **FTO-2** and **FTO-3**. This material is available free of charge via the Internet at http://pubs.acs.org.

■ AUTHOR INFORMATION

Corresponding Authors

*E-mail: mlwaters@email.unc.edu (M.L.W.)
*E-mail: tjmeyer@unc.edu (T.J.M.).

Present Address

‡J.J.C. current address: Department of Chemistry, Brookhaven National Laboratory, Upton, NY 11973.

Author Contributions

§D.M.R. and M.K.C. contributed equally.

Notes

The authors declare no competing financial interest.

■ ACKNOWLEDGMENTS

This research was primarily supported by the UNC EFRC: Center for Solar Fuels, an Energy Frontier Research Center (EFRC), funded by the U.S. Department of Energy (DOE), Office of Science, Office of Basic Energy Sciences, under Award DE-SC0001011 supporting D.M.R., J.J.C., Z.F., L.A., and D.M. Funding by the Center for Catalytic Hydrocarbon Functionalization, an EFRC, funded by the U.S. DOE, Office of Science, Office of Basic Energy Sciences, under Award DE-SC0001298 supporting M.K.C. is gratefully acknowledged. D.L.A. acknowledges support from a fellowship from the Department of Energy Office of Science Graduate Fellowship Program (DOE SCGF), made possible, in part, by the American Recovery and Reinvestment Act of 2009, administered by ORISE-ORAU under Contract DE-AC05-06OR23100.

■ REFERENCES

(1) Song, W.; Chen, Z.; Brennaman, M. K.; Concepcion, J. J.; Patrocinio, A. O. T.; Murakami Iha, N. Y.; Meyer, T. J. *Pure Appl. Chem.* **2011**, *83*, 749−768.

(2) Zhao, Y.; Swierk, J. R.; Megiatoo, J. D., Jr.; Sherman, B.; Youngblood, W. J.; Qin, D.; Lentz, D. M.; Moore, A. L.; Moore, T. A.; Gust, D.; Mallouk, T. E. *Proc. Natl. Acad. Sci. U.S.A.* **2012**, *109*, 15612−15616.

(3) Gao, Y.; Ding, X.; Liu, J.; Wang, L.; Lu, Z.; Li, L.; Sun, L. *J. Am. Chem. Soc.* **2013**, *135*, 4219−4222.

(4) Lapides, A. M.; Ashford, D. L.; Hanson, K.; Torelli, D. A.; Templeton, J. L.; Meyer, T. J. *J. Am. Chem. Soc.* **2013**, *135*, 15450−15458.

(5) Torelli, D. A.; Harrison, D. P.; Lapides, A. M.; Meyer, T. J. *ACS Appl. Mater. Interfaces* **2013**, *5*, 7050−7057.

(6) Hanson, K.; Torelli, D. A.; Vannucci, A. K.; Brennaman, M. K.; Luo, H.; Alibabaei, L.; Song, W.; Ashford, D. L.; Norris, M. R.; Glasson, C. R. K.; Concepcion, J. J.; Meyer, T. J. *Angew. Chem., Int. Ed.* **2012**, *51*, 12782−12785.

(7) Young, K. J.; Martini, L. A.; Milot, R. L.; Snoeberger, R. C., III; Batista, V. S.; Schmuttenmaer, C. A.; Crabtree, R. H.; Brudvig, G. W. *Coord. Chem. Rev.* **2012**, *256*, 2503−2520.

(8) Frischmann, P. D.; Mahata, K.; Würthner, F. *Chem. Soc. Rev.* **2013**, *42*, 1847−1870.

(9) Kärkäs, M. D.; Johnston, E. V.; Verho, O.; Åkermark, B. *Acc. Chem. Res.* **2014**, *47*, 100−111.

(10) Farràs, P.; Maji, S.; Benet-Buchholz, J.; Llobet, A. *Chem.—Eur. J.* **2013**, *19*, 7162−7172.

(11) Hamelin, O.; Guillo, P.; Loiseau, F.; Boissonnet, M.-T.; Menage, S. *Inorg. Chem.* **2011**, *50*, 7952−7954.

(12) Song, W.; Glasson, C. R. K.; Luo, H.; Hanson, K.; Brennaman, M. K.; Concepcion, J. J.; Meyer, T. J. *J. Phys. Chem. Lett.* **2011**, *2*, 1808−1813.

(13) Ashford, D. L.; Stewart, D. J.; Glasson, C. R.; Binstead, R. A.; Harrison, D. P.; Norris, M. R.; Concepcion, J. J.; Fang, Z.; Templeton, J. L.; Meyer, T. J. *Inorg. Chem.* **2012**, *51*, 6428−6430.

(14) Ashford, D. L.; Song, W.; Concepcion, J. J.; Glasson, C. R. K.; Brennaman, M. K.; Norris, M. R.; Fang, Z.; Templeton, J. L.; Meyer, T. J. *J. Am. Chem. Soc.* **2012**, *134*, 19189−19198.

(15) Kaveevivitchai, N.; Chitta, R.; Zong, R.; El Ojaimi, M.; Thummel, R. P. *J. Am. Chem. Soc.* **2012**, *134*, 10721−10724.

(16) Li, F.; Jiang, Y.; Zhang, B.; Huang, F.; Gao, Y.; Sun, L. *Angew. Chem., Int. Ed.* **2012**, *51*, 2417−2420.

(17) Norris, M. R.; Concepcion, J. J.; Glasson, C. R. K.; Fang, Z.; Lapides, A. M.; Ashford, D. A.; Templeton, J. L.; Meyer, T. J. *Inorg. Chem.* **2013**, *52*, 12492−12501.

(18) Vairaprakash, P.; Ueki, H.; Tashiro, K.; Yaghi, O. M. *J. Am. Chem. Soc.* **2011**, *133*, 759−761.

(19) Stewart, J. M.; Young, J. D. *Solid-Phase Peptide Synthesis*, 2nd ed.; Pierce Chemical Co.: Rockford, IL, 1984.

(20) Merrifield, B. *Science* **1986**, *232*, 341−347.

(21) Kümin, M.; Sonntag, L.-S.; Wennemers, H. *J. Am. Chem. Soc.* **2007**, *129*, 466−467.

(22) Deber, C. M.; Bovey, F. A.; Carver, J. P.; Blout, E. R. *J. Am. Chem. Soc.* **1970**, *92*, 6191−6198.

(23) Serron, S. A.; Aldridge, W. S.; Fleming, C. N.; Danell, R. M.; Baik, M.-H.; Sykora, M.; Dattelbaum, D. M.; Meyer, T. J. *J. Am. Chem. Soc.* **2004**, *126*, 14506−14514.

(24) Striplin, D. R.; Reece, S. Y.; McCafferty, D. G.; Wall, C. G.; Friesen, D. A.; Erickson, B. W.; Meyer, T. J. *J. Am. Chem. Soc.* **2004**, *126*, 5282−5291.

(25) Cowan, P. M.; McGavin, S. *Nature* **1955**, *176*, 501−503.

(26) Hruby, V. J. *Conformation in Biology and Drug Design*; Academic Press: Orlando, FL, 1985; Vol 7.

(27) Sasisekharan, V. *Acta Crystallogr.* **1959**, *12*, 897−903.

(28) Woody, R. W. *Adv. Biophys. Chem.* **1992**, *2*, 37−79.

(29) Ma, D.; Bettis, S. E.; Hanson, K.; Minakova, M.; Alibabaei, L.; Fondrie, W.; Ryan, D. M.; Papoian, G. A.; Meyer, T. J.; Waters, M. L.; Papanikolas, J. M. *J. Am. Chem. Soc.* **2013**, *135*, 5250−5253.

(30) Concepcion, J. J.; Tsai, M.-K.; Muckerman, J. T.; Meyer, T. J. *J. Am. Chem. Soc.* **2010**, *132*, 1545−1557.

(31) Concepcion, J. J.; Jurss, J. W.; Norris, M. R.; Chen, Z.; Templeton, J. L.; Meyer, T. J. *Inorg. Chem.* **2010**, *49*, 1277−1279.

(32) Chen, Z.; Concepcion, J. J.; Luo, H.; Hull, J. F.; Paul, A.; Meyer, T. J. *J. Am. Chem. Soc.* **2010**, *132*, 17670−17673.

(33) McCafferty, D. G.; Friesen, D. A.; Danielson, E.; Wall, C. G.; Saderholm, M. J.; Erickson, B. W.; Meyer, T. J. *Proc. Natl. Acad. Sci. U.S.A.* **1996**, *93*, 8200−8204.

(34) Aldridge, W. S., III; Hornstein, B. J.; Serron, S.; Dattelbaum, D. M.; Schoonover, J. R.; Meyer, T. J. *J. Org. Chem.* **2006**, *71*, 5186−5190.
(35) Bard, A. J.; Faulkner, L. R. *Electrochemical Methods, Fundamentals and Applications*, 2nd ed.; John Wiley and Sons, Inc.: Hoboken, NJ, 2001.
(36) Chen, Z.; Concepcion, J. J.; Jurss, J. W.; Meyer, T. J. *J. Am. Chem. Soc.* **2009**, *131*, 15580−15581.
(37) Norris, M. R.; Concepcion, J. J.; Fang, Z.; Templeton, J. L.; Meyer, T. J. *Angew. Chem., Int. Ed.* **2013**, *52*, 13580−13583.
(38) Yan, S. G.; Hupp, J. T. *J. Phys. Chem.* **1996**, *100*, 6867−6870.
(39) van der Vegte, E. W.; Hadziioannou, G. J. *J. Phys. Chem. B* **1997**, *101*, 9563−9569.
(40) Zaban, P.; Ferrere, S.; Gregg, B. A. *J. Phys. Chem. B* **1998**, *102*, 452−460.
(41) Qu, P.; Meyer, G. J. *Langmuir* **2001**, *17*, 6720−6728.
(42) Norris, M. R.; Concepcion, J. J.; Harrison, D. P.; Binstead, R. A.; Ashford, D. L.; Fang, Z.; Templeton, J. L.; Meyer, T. J. *J. Am. Chem. Soc.* **2013**, *135*, 2080−2083.
(43) Concepcion, J. J.; Jurss, J. W.; Hoertz, P. G.; Meyer, T. J. *Angew. Chem., Int. Ed.* **2009**, *48*, 9473−9476.
(44) Chen, Z.; Concepcion, J. J.; Hull, J. F.; Hoertz, P. G.; Meyer, T. J. *Dalton Trans.* **2010**, *39*, 6950−6952.

dx.doi.org/10.1021/ic5011488 | *Inorg. Chem.* 2014, 53, 8120−8128